ORIGINAL RESEARCH

Graphene Oxide Functionalized Gelatin Methacryloyl Microgel for Enhanced Biomimetic Mineralization and in situ Bone Repair

Ximing Peng[1,]*, Xin Liu[2,]*, Yanqing Yang[1,]*, Mingwei Yu[1], Zhiwei Sun[1], Xiangru Chen[1], Keqiang Hu[1], Jing Yang[1], Shaotang Xiong[2], Bin Wang[2], Liya Ma[3], Zhenxing Wang[4], Hanxiao Cheng[5,]*, Chuchao Zhou 🔟[1,]*

[1]Department of Plastic Surgery, Tongren Hospital of Wuhan University (Wuhan Third Hospital), Wuhan, 430060, People's Republic of China; [2]Medical Aesthetic Department, The Second People's Hospital of China Three Gorges University, The Second People's Hospital of Yichang, Yichang, Hubei, People's Republic of China; [3]The Centre of Analysis and Measurement of Wuhan University, Wuhan University, Wuhan, 430072, People's Republic of China; [4]Department of Plastic Surgery, Union Hospital, Tongji Medical College, Huazhong University of Science and Technology, Wuhan, 430022, People's Republic of China; [5]Department of Plastic Surgery, Hangzhou First People's Hospital, Hangzhou, Zhejiang, 310006, People's Republic of China

*These authors contributed equally to this work

Correspondence: Hanxiao Cheng; Chuchao Zhou, Email chxmomo@sina.com; chuchaozhou@163.com

Introduction: The formation of bone-like apatite (Ap) on natural polymers through biomimetic mineralization using simulated body fluid (SBF) can improve osteoconductivity and biocompatibility, while lowering immunological rejection. Nonetheless, the coating efficiency of the bone-like Ap layer on natural polymers requires improvement. Carbonyls (-COOH) and hydroxyls (-OH) are abundant in graphene oxide (GO), which may offer more active sites for biomimetic mineralization and promote the proliferation of rat bone marrow stromal cells (BMSCs).

Methods: In this study, gelatin methacryloyl (GelMA) microgels were infused with GO (0, 0.5, 1, and 2 mg/mL) and embedded into microgels in SBF for 1, 7, and 14 days. Systematic in vitro and in vivo experiments were performed to evaluate the structure of the microgel and its effect on cell proliferation and ability to repair bone defects in rats.

Results: The resulting GO-GelMA-Ap microgels displayed a porous, interconnected structure with uniformly coated surfaces in bone-like Ap, and the Ca/P ratio of the 1 mg/mL GO-GelMA-Ap group was comparable to that of natural bone tissue. Moreover, the 1 mg/mL GO-GelMA-Ap group exhibited a greater Ap abundance, enhanced proliferation of BMSCs in vitro and increased bone formation in vivo compared to the GelMA-Ap group.

Discussion: Overall, this study offers a novel method for incorporating GO into microgels for bone tissue engineering to promote biomimetic mineralization.

Keywords: graphene oxide, gelatin methacryloyl, bone-like apatite, biomimetic mineralization, simulated body fluid, bone repair

Introduction

Large bone defects resulting from trauma, infection, or tumor excision contribute to a worldwide clinical issue,[1] particularly in their reconstruction and repair. Bone defect repair can be divided into three main categories: autografts, allografts, and artificial bone microgels.[2] Meanwhile, in the field of bone reconstruction, autografts are the gold standard for offering optimal osteoconductive, osteoinductive, and osteogenic properties. Nonetheless, this technique is plagued with complications, such as insufficient bone mass, irreparable donor site damage, and low availability, thus, restricting the application of autografts bone tissue reconstruction.[3] Similarly, allograft utilization is limited by the possible risk of disease transmission and immunological rejection. Consequently, there is an urgent requirement to create optimum artificial bone substitutes for bone regeneration.

6725

Graphical-Abstract
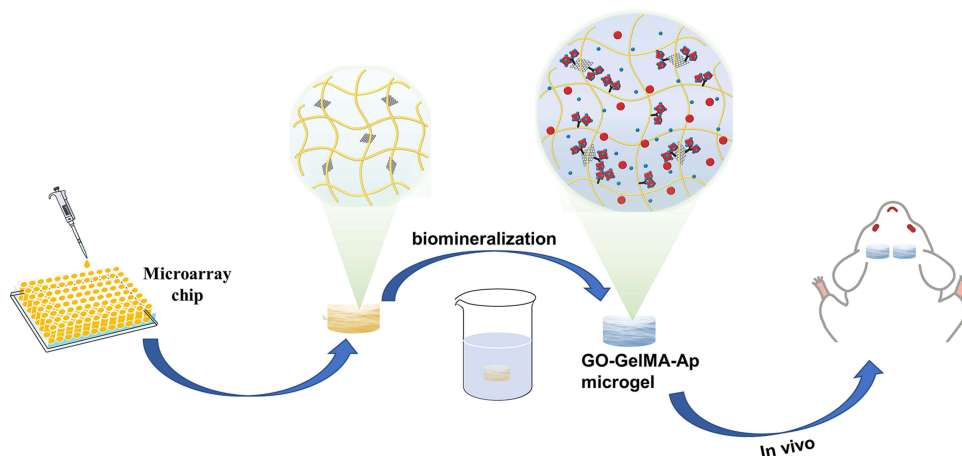
A number of artificial bone substitutes have been developed in recent years, such as those made of hydrogels, nanoparticles, nanofilms, nanocomposites, etc.[4] Hydrogels, resembling the natural ECM, are optimal for recreating conditions for in vitro cell culture and provide three-dimensional (3D) support for tissue formation.[5] Furthermore, hydrogels are promising in bone regeneration due to tunable mechanical strength, favorable biocompatibility, and good bioactivity. In this regard, naturally occurring hydrogel-based biopolymers may be superior to synthetic polymers due to their vast availability, low cost, good immunogenicity, cytocompatibility, and degradability under physiological conditions. At present, hydrogels are primarily divided into alginate, chitosan, gelatin/GelMA, hyaluronic acid, fibrinogen, collagen, and zein. Among them, Gelatin methacryloyl (GelMA) is one of the most promising biomaterials due to its low antigenicity, high solubility, less immunogenicity, and ease of UV cross-linking.[6,7] Recently, GelMA has been extensively applied as a microgel in the reconstruction of bones because of the outstanding biocompatibility and surface modification ability. The GelMA microgel can be easily modified, cross-linked, or coated with other bioactive molecules to create biological microgels with customized biological properties, including excellent mechanical properties, superior biodegradation properties, controlled drug release.[8,9] Moreover, the unique microstructure of GelMA microgel is conductive to cell proliferation, migration, and differentiation.[10] Despite that, the mechanical strength and osteoconductivity of the GelMA microgel require further improvements.[11]

For the past few years, carbon nanotubes (CNTs), graphene oxide (GO), and carbon nano-onions (CNOs) were integrated into gelatin to enhance the mechanical and biological properties of gelatin-based microgels.[12] Among these materials, GO is considered the most promising carbon material for bone regeneration due to its high surface area, superior antimicrobial properties and biocompatibility. Recent research has also demonstrated graphene oxide (GO) is a suitable nanomaterial for enhancing the mechanical characteristics of microgel.[13] Functional groups, such as the carbonyls (-COOH) and hydroxyls (-OH), are abundant in GO and could generate chemical connections with hydrogels and accelerate MSC osteogenic differentiation to different degrees. The GO π-π bonds could also adsorb proteins and ions to promote stem cell differentiation and proliferation.[14] Nonetheless, the inefficient osteoconductivity of these GO-based microgels poses a challenge for practical application.[15]

In recent years, many scholars have found that in addition to the surface morphology, the material composition at the interface also affects the cell fate.[16] Hydroxyapatite (Ap) is a product of biomimetic mineralization using simulated body fluids (SBFs) and has become a common bone substitute due to the excellent biocompatibility, osteoconductivity, and osteoinductivity, and the similarity between the inorganic component with human and animal bones.[17] The morphology structure and crystalline structure of Ap are essential in involving in mediating cellular behavior. For instance, the Ap crystalline structure influences the release of calcium (Ca) and phosphate (P) ions, determining cell fate. It has been

found that Ap can be incorporated into nanomaterials and nanofiber to enhance the osteoinductive and osteoimmuno-modulatory functions of the fiber scaffolds.[9,18,19] Furthermore, the Ap morphology could provide biophysical informa-tion to adjust cell behaviors, while the surface roughness could promote cell adhesion and proliferation.[20]

In this study, mineralized GO-GelMA-Ap microgels were prepared using a microarray chip, followed by mineraliza-tion in SBF to form the Ap layer. Systematic in vitro experiments were carried out to estimate the uniformity of Ap distribution in the microgel and assess the influence of the microgel on both cell proliferation and osteogenic differentia-tion. Moreover, the in vivo validation was conducted to ascertain the microgel capacity to regenerate bone tissues in a rat calvarial defect model. The study findings demonstrated that GO-GelMA-Ap could repair the calvaria critical-size bone defect, and 1 mg/mL GO-GelMA-Ap microgel was superior in repairing the calvaria critical-size bone defect.

Materials and Methods

Graphene (500 meshes) was obtained from Acros Organic Company (USA). Reagents sodium chloride (NaCl), sodium bicarbonate (NaHCO$_3$), potassium chloride (KCl), potassium hydrogen phosphate trihydrate (K$_2$HPO$_4$·3H$_2$O), Magnesium chloride hexahydrate (MgCl$_2$·6H$_2$O), hydrochloric acid (HCl), calcium chloride (CaCl$_2$), sodium sulfate anhydrous (Na$_2$SO$_4$), and tris(hydroxymethyl)aminomethane [CNH$_2$(HOCH$_2$)$_3$] were obtained from Sinopharm Chemical Reagent Co., Ltd. Kokubo's method was used to prepare SBF solution.[21]

Phosphate-buffered saline (PBS) and trypsin−EDTA were obtained from Servicebio technology Co., Ltd. Fetal bovine serum (FBS), low-glucose Dulbecco's modified Eagle's medium (L-DMEM), 1% penicillin and streptomycin were obtained from Hyclone.

The study was performed in compliance with the Guide for the Care and Use of Laboratory Animals from the National Institutes of Health and approved by the Committee on Ethics of Animal Experiments of Tongren Hospital of Wuhan University. The experimental protocol was formally approved by the Ethics Committee of Wuhan Third Hospital, Tongren Hospital of Wuhan University, and observed the Guideline for the Care and Use of Laboratory Animals.

Fabrication of the GO−GelMA-Ap Microgels
Synthesis of GO−GelMA−Ap Microgels

The modified Hummer method was used to prepare GO. First, a mixture of phosphoric and sulfuric acid was prepared at a ratio of 1:9. A mixture of potassium permanganate, and graphene (6:1) was then added to the acid mixture in an ice bath and heated at 50°C for 12 hours with constant stirring. Subsequently, 30% hydrogen peroxide (H$_2$O$_2$) was added to obtain GO with a higher oxidation level and a more regular structure.[22] GelMA was produced by directly reacting gelatin with MA in a phosphate buffer solution (pH = 7.4) at 50°C, adding methacryloyl substitution groups onto the amino acid residues of reactive amine and hydroxyl groups.[23] Laser prototyping is a new technology to prepare the micro-stencil array chip using polymethyl methacrylate (PMMA).[24] The GO−GelMA−Ap microgels were synthesized by chemical cross-linking and biomimetic mineralization (Figure 1). First, 20% GelMA and GO [0%, 0.1%, 0.2%, 0.4% w/v in 20 mL phosphate-buffered saline (PBS)] solutions were mixed at a ratio of 1:1 (GO final concentrations: 0%, 0.05%, 0.1%, and 0.2% w/v) under sonication for 15 min. The resulting solutions were cast in a micro mold plate (length: 7.5 cm, width: 2.5 cm, height: 0.01 cm). After cross-linking the micro-mold plates under UV light at a wavelength of 365 nm, the microgels were collected in six-well plates and lyophilized for 12 h to obtain microspheres (diameter: 1500 um, height: 1 mm). The steps were repeated for GO microgel fabrication. The composite microgels were soaked in CaCl$_2$ and K$_2$HPO$_4$ solutions to accelerate the process of depositing biomimetic apatite. Subsequently, the microgels were immersed in a 20 mL solution containing 0.2 M CaCl$_2$ for a duration of 3 min, followed by 20 mL of deionized water for 3 s, 20 mL solution containing 0.2 M K$_2$HPO$_4$ for 3 min, and 20 mL of deionized water for 3 s. These steps were repeated thrice in this experiment. As the microgel was immersed in 40 mL SBF, Ap was gradually deposited on the microgel surface. The microgels were stored at 37°C for several periods (1, 3, 5, and 7 days), and the SBF solution was changed daily to maintain an evenly distributed ionic strength throughout the experiment. Reagents NaCl, NaHCO$_3$, KCl, K$_2$HPO$_4$·3H$_2$O, MgCl$_2$·6H$_2$O, HCl, CaCl$_2$, Na$_2$SO$_4$, and [CNH$_2$(HOCH$_2$)$_3$] were dissolved in deionized water to prepare the SBF solution and adjusted to pH 7.40 at 36.5°C using Tris (hydroxymethyl) aminomethane and aqueous 1 M HCl
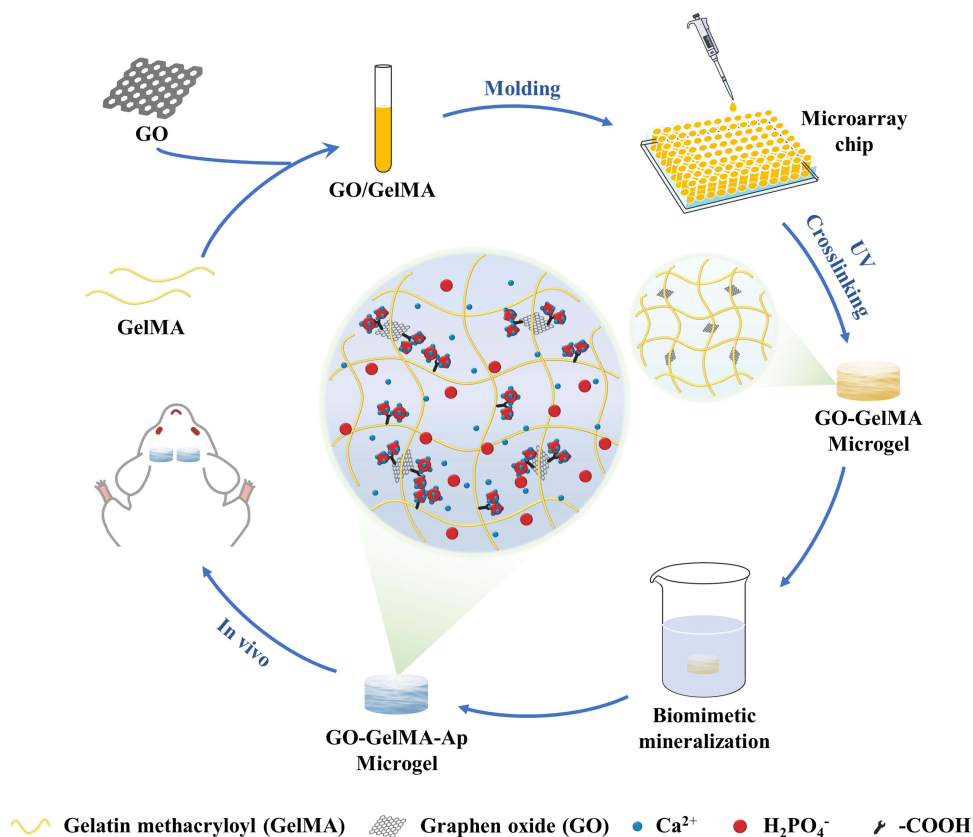
Figure 1 Schematic diagram of the synthesis of GO−GelMA−Ap microgels and application to cranial bone defect.

solution. The microgels were washed with deionized water once removed from the SBF and frozen at −50°C for 12 h under vacuum conditions.

Characterization of Microgels
Mass Increase (MI) of the Microgels After Biomimetic Apatite Deposition
The microgels' MI was measured following biomimetic Ap deposition in SBF using an electronic analytical balance with an accuracy of 10^{-5} g. The difference between M1 (microgel mass before alternate sedimentation in $CaCl_2$ and K_2HPO_4 solutions) and M2 (microgel mass after biomimetic Ap deposition) is described by eq. 1.

$$MI(\%) = \frac{M2 - M1}{M1} \times 100\% \qquad (1)$$

Environmental Scanning Electron Microscopy (ESEM) and Energy-Dispersive Spectrometry (EDS) Evaluation
The ESEM (Quanta 200, FEI Company, USA) was used to observe the morphology and microstructure of the microgels surface and cross-section pre- and post-biomimetic mineralization coating. Meanwhile, EDS was used to evaluate the ratio of calcium and phosphate in the biomimetic coating.

X-Ray Diffraction (XRD), Fourier Transform (FTIR), and Thermogravimetric Analysis (TGA) Evaluation
The XRD (Empyrean, PANalytical B.V.) was used to analyze the crystalline phases at a scanning rate of 0.013°/s in a 2θ range from 5° to 40° with Cu Kα radiation (Kα1= 1.540598 Kα2=1.544426). The FTIR spectroscopy instrument (VERTEX 70; Bruker) was applied to confirm functional groups on biomimetic mineralized microgels from 4000 to 400 cm^{-1} at a resolution of 0.4 cm^{-1}. The TGA (Diamond TG/DTA; Perki-nElmer Instruments, Shanghai, China) was used to measure the amount of Ap in the 3D microgels. In this experiment, the microgel was heated from 25°C to 800°C at a temperature of 50°C per minute in an N_2 atmosphere.

Mechanical Properties Evaluation and in vitro Degradation

An all-electric dynamic test instrument was used to evaluate the mechanical properties of the microgels at a loading rate of 5 mm/min until the strain reaches 20%. The mechanical characteristics of the microgels were assessed using an all-electric dynamic test equipment (ElectroPuls E1000, INSTRON) and the evaluation was conducted at a loading rate of 5 mm/min until the strain reaches 20%. Weight loss was used to show degradation of microgels. Initially weighed microgel specimens with different concentration (W_0) were immersed in collagenase solution and incubated for 12 hours at 37°C. Then, the samples were drawn out of the buffer solution at 3 hours, washed with distilled water, then dehydrated in the desiccator and weighed (W_t).[25]

The weight loss ratio calculated as $\frac{W0-Wt}{W0} \times 100\%$

The weight remaining ratio was calculated as

$$1 - [\frac{W0 - Wt}{W0} \times 100\%]$$

Micro-Computed Tomography (Micro-CT) Analysis

The Micro-CT (SkyScan1176; Bruker, German) was used to observe the Ap deposition. VG studio software (Volume Graphics GmbH, Heidelberg, Germany) was used to reconstruct the corresponding 3D images. The apatite volume (AV) and the proportion of apatite volume relative to total volume (AV/TV) were calculated using the Micro-CT assistance software (Scanco Medical, Zurich, Switzerland).

In vitro Cellular Evaluation

Rat Bone Marrow Stromal Cells (BMSC) Isolation and in vitro Culture

Rat BMSC were separated and extracted using the previously mentioned method.[26] Newborn Sprague Dawley rats (3 − 5 days old) were euthanized via cervical dislocation and soaked in 75% alcohol for 10 min. The long bones in their extremities were separated from attached muscles and soft tissues. Cartilage at both ends of the bones was extracted using ophthalmic scissors, and the treated cartilage was rinsed repeatedly using the culture medium until the cavities appeared white. In the end, a complete medium was used to grow fresh bone marrow tissues, which were later incubated in 5% carbon dioxide (CO_2) at 37°C. The culture medium was replaced every 5 days, and the BMSC passage was indicated by the fusion of the attached BMSCs.

Cell Seeding on Microgels

The microgels were disinfected in 75% alcohol for 20 min, rinsed thrice with PBS, and soaked in the medium overnight. The BMSC (passage 3) were digested with trypsin and re-suspended at a density of 1×10^6 cells/mL. Subsequently, 20 sterilized microgels were placed in a six-well plate (Corning Int., Singapore) and were seeded with 60 μL of cell suspension. After a 2 h incubation, the cell-seeded microgels were transferred into a new 6-well plate and cultured in 2 mL Dulbecco's modified eagle medium (DMEM, Hyclone). The cultures were maintained in an incubator in 5% CO_2 at 37°C, and the media were replaced every 3 days.

Assessment of Cell Viability, Proliferation and Migration

Living cells and dead cells were visualized by calcein AM and propidium iodide (PI) staining, respectively. Briefly, after 1, 3, and 7 days of incubation, the microgels were washed three times with phosphate-buffered saline (PBS) and subsequently soaked in calcein staining solution for 45 min and PI solution for 10 min at 37°C. Then the microgels were examined using confocal fluorescence microscopy. The cell-seeded microgels at specified time points (1, 3, and 7 d) were added in a 96-well plate. Then, 20 μL MTT solution and 200 μL complete medium were added in 96-well for 4 h incubation at 37°C in 5% CO_2 in darkness. Next, the microgels were washed with PBS and treated with 150 μL dimethyl sulfoxide (DMSO, Sigma, USA). Subsequently, DU 730 UV/Vis spectrophotometer (Beck-man Coulter, USA) was applied to record absorbance at 450 nm wavelength.

In vivo Evaluation of Cranial Defect

In situ Bone Regeneration of Rat Cranial Defect

To investigate the potential of the GO−GelMA−Ap implants in promoting new bone formation in vivo, a total of 24 female adult SD rats (6 weeks old, weighing between 170 and 230 g) were obtained from the Animal Management Center of Wuhan Third Hospital, Tongren Hospital of Wuhan University and were randomly divided into four groups: (1) GelMA; (2) 0.5 mg/mL GO−GelMA−Ap; (3) 1 mg/mL GO−GelMA−Ap; and (4) 2 mg/mL GO−GelMA−Ap (n = 6 rats per group). The 10% chloral hydrate was injected to narcotize the rats and rats were sagitally incised 2 cm down the middle of the scalp. The rat fascia was isolated and cleaned to expose the calvaria, and the cranial defect was drilled in two parallel directions 5 mm apart. Ultimately, microgels were implanted to close the incision in the defect area. Implanted specimens were gained at 4 weeks and 12 weeks post-operation. New bone formation was evaluated with a Micro-CT scanner (SkyScan 1176; Broker). Calculations were conducted using CTAn software to determine bone volume/tissue volume (BV/TV) and bone mineral density (BMD).

Histological Observation

Staining of the samples obtained at 12 weeks was preceded by 7 days of paraformaldehyde fixation and 4 weeks of decalcification in 10% Ethylene Diamine Tetraacetic Acid (EDTA). After decalcification, the samples were dehydrated in a graded ethanol series, embedded in paraffin, and sectioned with a thickness of 2mm. Staining of the divided samples with HE and Masson's Trichrome (Sigma, USA) and microscope observation (Eclipse Ni-E; Tokyo, Japan) were carried out. OCN monoclonal antibodies (Abcam, UK) were incubated separately on the processed sections after being blocked for 30 minutes with ghost serum antibody. Finally, the staining samples were examined under the microscope.

Statistical Analysis

All data presented in this study are expressed as the mean ± SD. Student's *t*-test was used to compare the means of two groups and one-way analysis of variance (ANOVA) tests with post hoc contrasts by Student−Newman−Keuls test was used to compare the means of multiple groups. $P < 0.05$ was considered to be a statistically substantial difference.

Results

Macro- and Micro Images of Microgels Before Biomimetic Apatite Deposition

The GelMA microgel was white, while the other three GO−GelMA microgels with GO concentration from 0.05% to 0.2% w/v exhibited a gradual color change gradually from brown to black (Figure 2A). The surface and cross section morphology of the microgels before bio was illustrated in SEM images. All four microgels groups demonstrated porous and interconnected structures. Meanwhile, the surface of the GelMA microgel was smooth, and the other three GO−GelMA microgels were folded and had uneven surfaces. The cross-sectional observation also indicated a smooth morphology of the GelMA microgel and rougher surfaces on the GO-incorporated microgels (Figure 2B).

SEM Images of the Surface and Cross-Section of the Microgels After Biomimetic Apatite Deposition

On the third day of mineralization, the Ap crystal attachment was observed in the surface and cross-section of all microgels with uneven mineral distribution (Figure 3A). Moreover, increased mineralized crystallization was observed in relation to prolonged mineralization time and GO concentration increment. The 1 mg/mL GO-GelMA group possessed the most mineralized crystals when the SBF immersion time was extended to day 7 (Figure 3B).

Characterization of Microgels

Based on the earlier findings, in vitro and in vivo experiments were carried out with a seven-day SBF treatment. According to the EDS analysis, most of the minerals on the microgels contain calcium and phosphorus, with Ca/P ratios estimated (Figure 4A). The Ca/P ratio (1.66 ± 0.066) in the GO−GelMA−Ap group with a concentration of 1 mg/mL exhibited the highest similarity to natural bone tissue (1.67). The distribution of Ca and P elements on the microgels was slightly uneven, as confirmed by the EDS
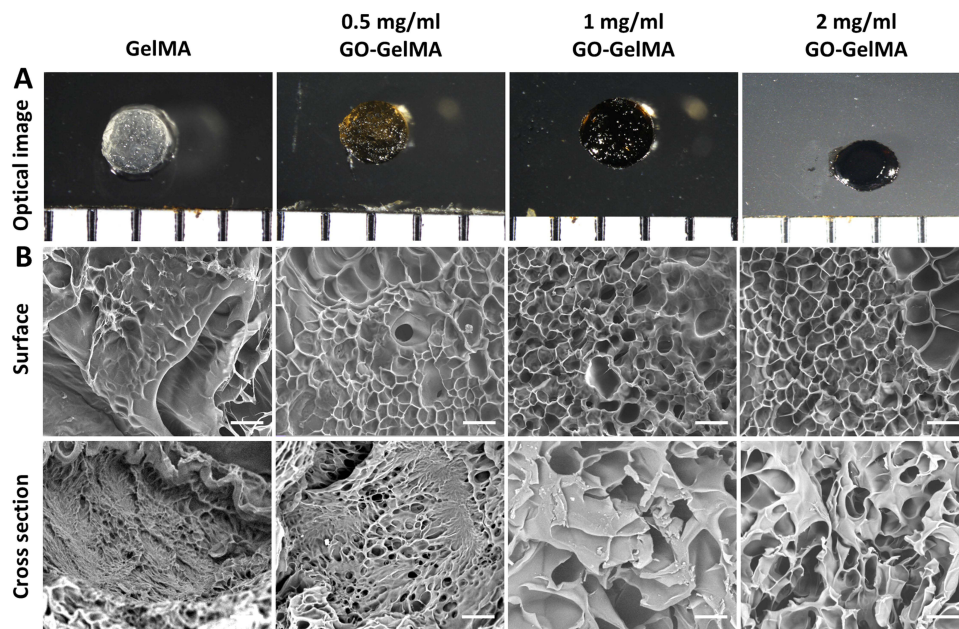
Figure 2 Optical and SEM image of the microgels before biomineralization. (**A**) Optical image of GelMA, 0.5, 1, and 2 mg/mL GO-GelMA microgels; (**B**) surface and cross section SEM image of the microgels before biomineralization. Scale bar = 20 μm.
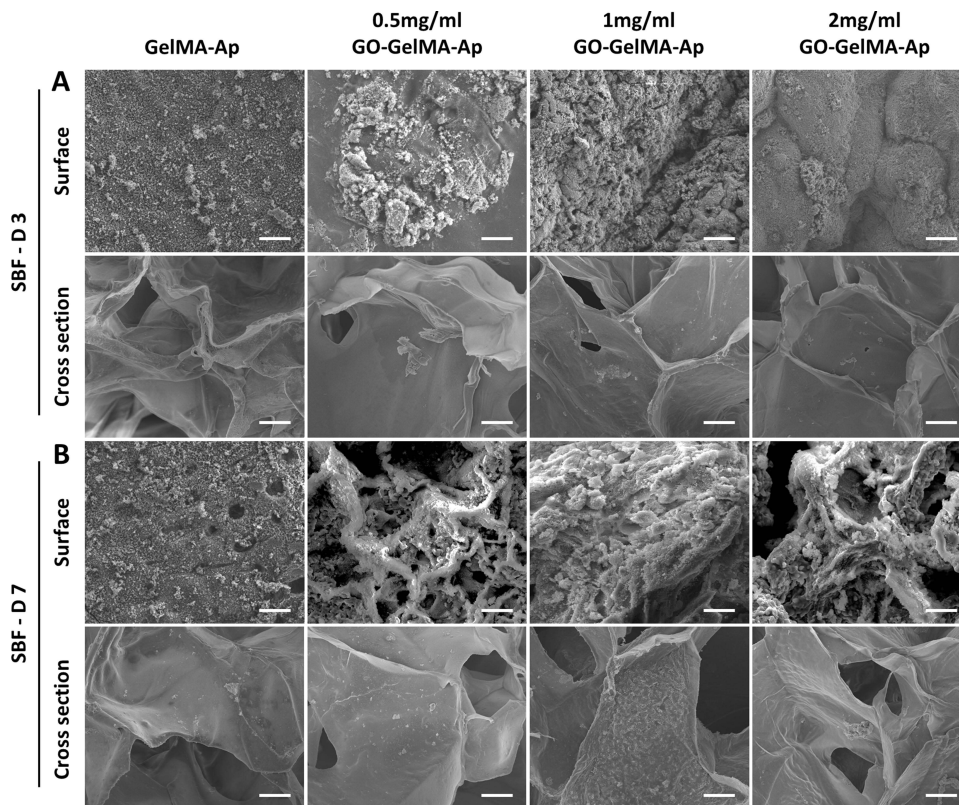

Figure 3 Surface and cross-sectional SEM images of the microgels after biomineralization for 3 and 7 days. Scale bar = 10 μm (**A** and **B**).

mapping (Figure 4B), potentially attributed to the irregular morphology of the microgel surface. Mineral formation on the microgel surface was analyzed using X-ray diffraction measurements (Figure 4C). For GO, the 2θ peak can be seen to be shifted to 9.03°, which indicated that the graphene was fully oxidized into GO.[27] The characteristic absorption peaks of Ap were
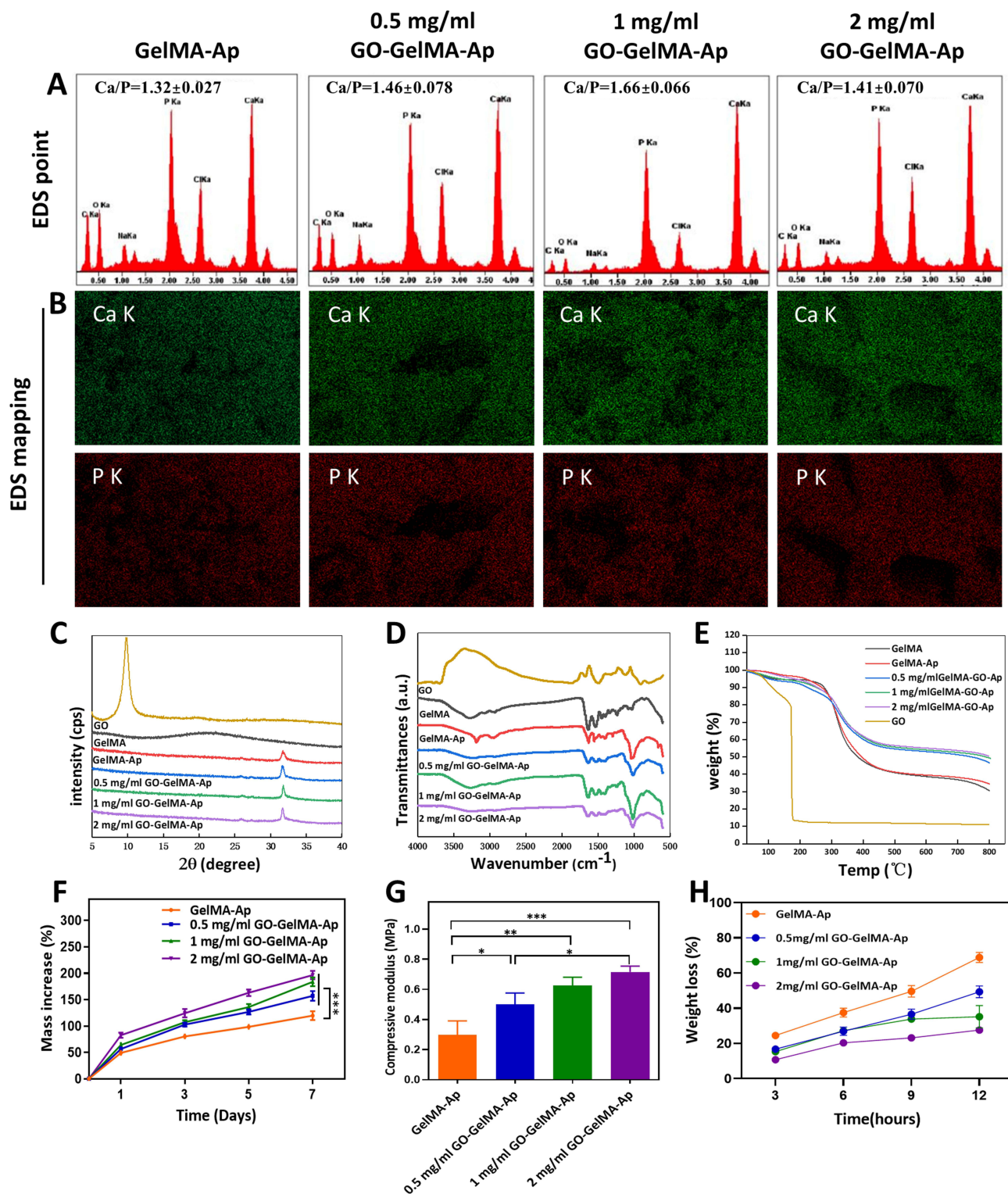
Figure 4 Characterization of the microgels. (**A**) The EDS point assessment of the composite microgel; (**B**) the EDS mapping assessment of the composite microgel; (**C**) XRD spectra; (**D**) FTIR spectra; (**E**) TGA analysis of the microgels; (**F**) mass increase percentage; (**G**) compressive modulus of the microgels after biomineralization in SBF; (**H**) in vitro degradation of microgels. * $p < 0.05$, ** $p < 0.01$, *** $p < 0.001$.

observed at $2\theta = 26°$ and $2\theta = 32°$ in all four groups of mineralized microgels when compared with the GelMA microgel.[28] Moreover, there was a significant rise in the absorption peak with the increase in GO concentration. The microgel chemical composition was analyzed using FTIR spectroscopy ([Figure 4D](#)). FTIR spectrum of GO exhibited various oxygenated bands at

3385 cm^{-1}, which are assigned to O-H vibrations.[29] The GelMA microgels showed a distinct gelatine amide band; the peak at 3310 cm^{-1} corresponded to the N-H stretch of amide A, the peak at 3063 cm^{-1} corresponded to the C-H stretch of amide B, the peak at 1629 cm^{-1} corresponded to the C=O stretch of amide I, the peak at 1539 cm^{-1} corresponded to the N-H deformation of amide II, and the peak at 1235 cm^{-1} corresponded to the N-H deformation of amide III.[30] In the biomimetic mineralized microgels, the peaks at 1033cm^{-1}, 961cm^{-1}, and 601 cm^{-1} corresponded to the vibration of the PO$_4^{3-}$ groups of Ap, indicating the formation of carbon-hydroxyapatite during mineralization, which is similar to natural bone Ap.[31]

After biomimetic mineralization, the microgel mineral content was determined by thermogravimetric analysis (Figure 4E). The remaining weights of GO, GelMA, GelMA−Ap, 0.5 mg/mL GO−GelMA−Ap, 1 mg/mL GO−GelMA−Ap, and 2 mg/mL GO−GelMA−Ap microgels were 10.97%, 30.77%, 34.46%, 46.75%, 49.32%, and 50.12%, respectively. The sharp decrease of GO from 190°C to 200°C was related to the overflow of GO in that temperature range.[32] These results indicated more Ap was deposited in 1 mg/mL and 2 mg/mL GO−GelMA−Ap groups. The rate of increase in microgel weight was determined by analyzing the weight changes during the mineralization process, and the Ap content in the microgels was also analyzed (Figure 4F). There were significant differences ($p < 0.05$) between all microgels at day 7 (GelMA−Ap, 119.8% ± 8.4%; 0.5 mg/mL GO−GelMA−Ap, 157.0% ± 9.1%; 1 mg/mL GO−GelMA−Ap, 183.7% ± 8.17%; 2 mg/mL GO−GelMA−Ap, 196.5% ± 8.0%). The mechanical properties of the microgels were evaluated via a compression test (Figure 4G). According to the findings, it was observed that the elastic modulus of GelMA−Ap microgels (45.28 ± 4.01 KPa) exhibited a significantly reduced value in comparison to the microgels incorporated with GO (0.5 mg/mL GO−GelMA−Ap, 65.19 ± 12.27 KPa; 1 mg/mL GO−GelMA−Ap, 94.96 ± 2.76MPa; and 2 mg/mL GO−GelMA−Ap, 138.6 ± 12.27KPa). In vitro, collagenase degradation was performed on all microgels (Figure 4H) and the degradation rates of GelMA, GelMA−Ap, 0.5 mg/mL GO−GelMA−Ap, 1 mg/mL GO−GelMA−Ap, and 2 mg/mL GO−GelMA−Ap microgels within 12 h were 68.9% ± 2.8%, 49.4% ± 3.3%, 35.1% ± 6.3%, 27.6% ± 1.7%, respectively.

Micro-Computed Tomography (Micro-CT) Analysis of Microgels

The Ap content and proportion of all microgels were analyzed using Micro-CT. Based on the cross-section (Figure 5A), the Ap is mainly distributed on the microgel surface. Furthermore, the 1 mg/mL and 2 mg/mL GO-GelMA-Ap microgels had more hydroxyapatite content and better mineralization at the central position from the coronal view (Figure 5B). The Ap volume (AV) quantitative calculation of the four microgel groups is 0.317 ± 0.010, 0.570 ± 0.044, 1.107 ± 0.031, 1.344 ± 0.064 mm^3, respectively (Figure 5C). The Ap volume in microgels with GO was higher than the GelMA microgels, which increased with GO concentration. The percentages of Ap volume in the total volume (AV/TV) of the four microgel groups are 2.842 ± 0.386%, 6.407 ± 1.371%, 12.830 ± 0.647%, and 15.340 ± 0.897%, respectively (Figure 5D). The Ap proportion in microgels with GO was higher than in GelMA microgels, and 2 mg/mL GO-GelMA-Ap microgel recorded the largest overall volume fraction.

In vitro Cellular Evaluation of the Microgels

Confocal laser microscopy was used to assess the BMSC survival and dispersion on the microgels at days 1, 3, and 7 post-seeding and analyzed in three dimensions (Figure 6A). Live and dead cell staining was performed to observe the cell survival on the microgels. On the first day, few viable cells were evident on the microgels of the four groups. After incubating for 3 days, the SEM was performed to assess the cellular morphologies within the microgels. Fewer single cell appeared on the surface of the microgels in GelMA−Ap and 0.5 mg/mL GO−GelMA−Ap groups. Conversely, more clustered cells were present in 1 mg/mL and 2 mg/mL GO−GelMA−Ap groups (Figure 6B). At day 7, the number of living cells revealed the cell growth rate was remarkably higher in the 2 mg/mL GO−GelMA−Ap microgel (Figure 6C). Finally, the MTT assay assessed cell proliferation in the microgels on day 1, 3, and 7. Thus, it can be inferred that the 1 and 2 mg/mL GO−GelMA−Ap group has a higher proliferation rate on days 3 and 7 (Figure 6D).

In vivo Evaluation of Microgels

Rat Cranial Bone Defect Model

The rat cranial bone defect model was established to assess the new bone-forming abilities of four microgels and examine the osteogenic capacity of the microgels. These microgels were implanted into 5 mm critical-sized bone lesions. Micro-CT was
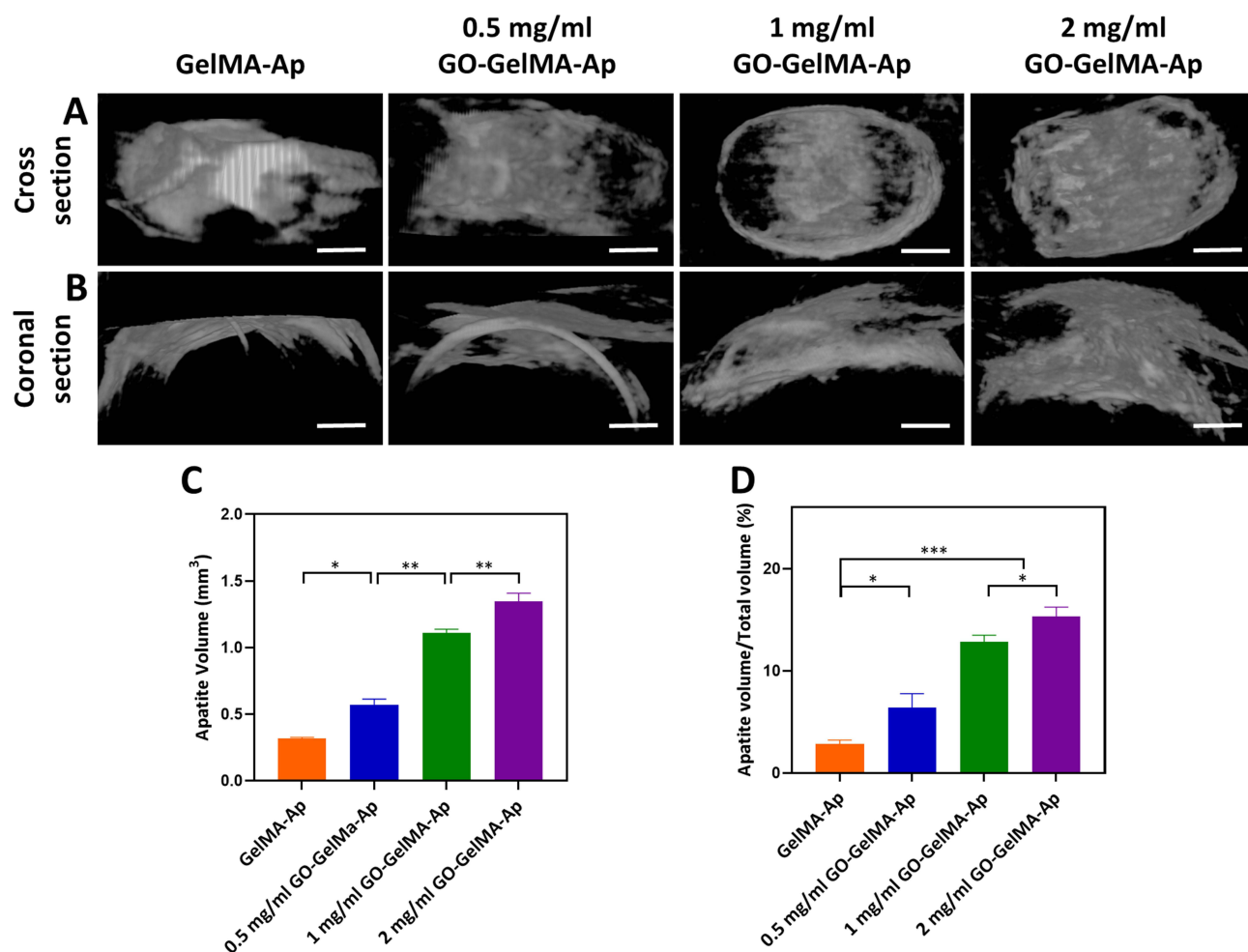
Figure 5 Micro-CT analysis of the microgels. (**A**) cross-section and (**B**) coronal section images of microgels. Scale bar = 500 μm. (**C**) Apatite volume (AV) and (**D**) the apatite volume fraction (AV/TV) of microgels. * $p < 0.05$, ** $p < 0.01$, *** $p < 0.001$.

employed to conduct the 3D reconstruction pictures of freshly produced bones at weeks 4 and 12 post-implantation (Figure 7A and B). The borders of the lesions exhibited the growth of newly-formed bones in all groups, while a section of new bone formation was evident in the central area of the defects of the 1 mg/mL and 2 mg/mL GO-GelMA-Ap microgels at week 4 post-implantation. Meanwhile, the cranial bone deficiencies in the 1 mg/mL GO-GelMA-Ap microgel were almost completely filled with freshly generated, thick bone tissue during 12 weeks. In addition, the 1 mg/mL GO-GelMA-Ap group had significantly greater ratios of new bone tissue volume fraction (BV/TV) and bone mineral density (BMD) at week 12 post-implantation, according to the micro-CT quantitative analysis (Figure 7C and D).

Histological Analysis of Bone Regeneration

Hematoxylin and eosin (H&E) staining and Masson's trichrome staining (Figure 8A–D) of the microgels at 12 weeks post-implantation demonstrated bone lacunas, as well as central canals could be observed in the four groups. Notably, bone lacuna contained more new bone tissue in the 1 mg/mL GO−GelMA-Ap group than in the other groups. Following 12 weeks of implantation, the margins of the four groups exhibited an appearance of dense and developed bone tissues, as shown by H&E staining and Masson's trichrome staining. Most of dense bone tissue is distributed at the defects in 1 mg/mL GO−GelMA−Ap group, contrary to the other groups. The OCN expression was immunohistochemically determined after 12 weeks of implantation to assess the osteogenic ability of the microgels. A positive OCN expression (Figure 9) was indicated by the brown areas surrounding the implants. At 12 post-implantation, more new bone tissues
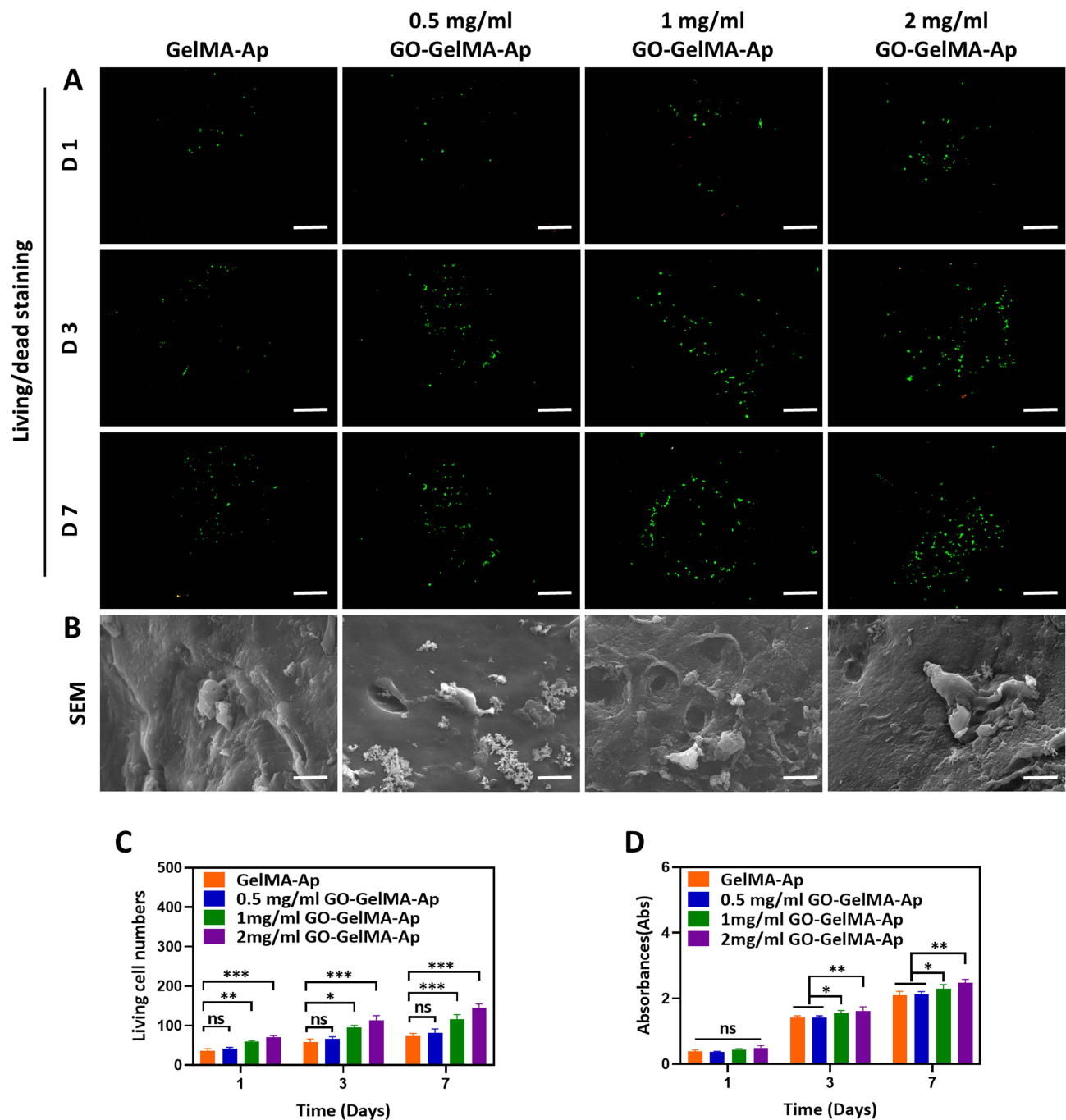
Figure 6 In vitro cellular evaluation of the microgels. (**A**) Confocal microscopy imaging of BMSC cultured on the microgels with calcein AM/PI staining at day 1, 3 and 7. Scale bar = 500 μm; (**B**) the SEM image of BMSC culture on the microgels at day 3. Scale bar = 10 μm; (**C**) the living cell numbers of the microgels at day 1, 3, and 7; (**D**) the MTT analysis of the microgels at day 1, 3, and 7. * $p < 0.05$, ** $p < 0.01$, *** $p < 0.001$.

and brown positive signals were distributed in the 1 mg/mL GO-GelMA−Ap group. The brown positive signals suggested the new bone tissue regeneration in 1 mg/mL GO-GelMA-Ap group.

Discussion

Biomimetic mineralization to deposit Ap onto the surfaces of microgels using SBF is a common technique to enhance the osteoconductive capacity of the bone graft alternatives.[33] Nonetheless, this method lacks the efficiency in producing an evenly distributed and substantial bone-like Ap covering on the microgel surfaces.[34] Therefore, a biomimetic GO-
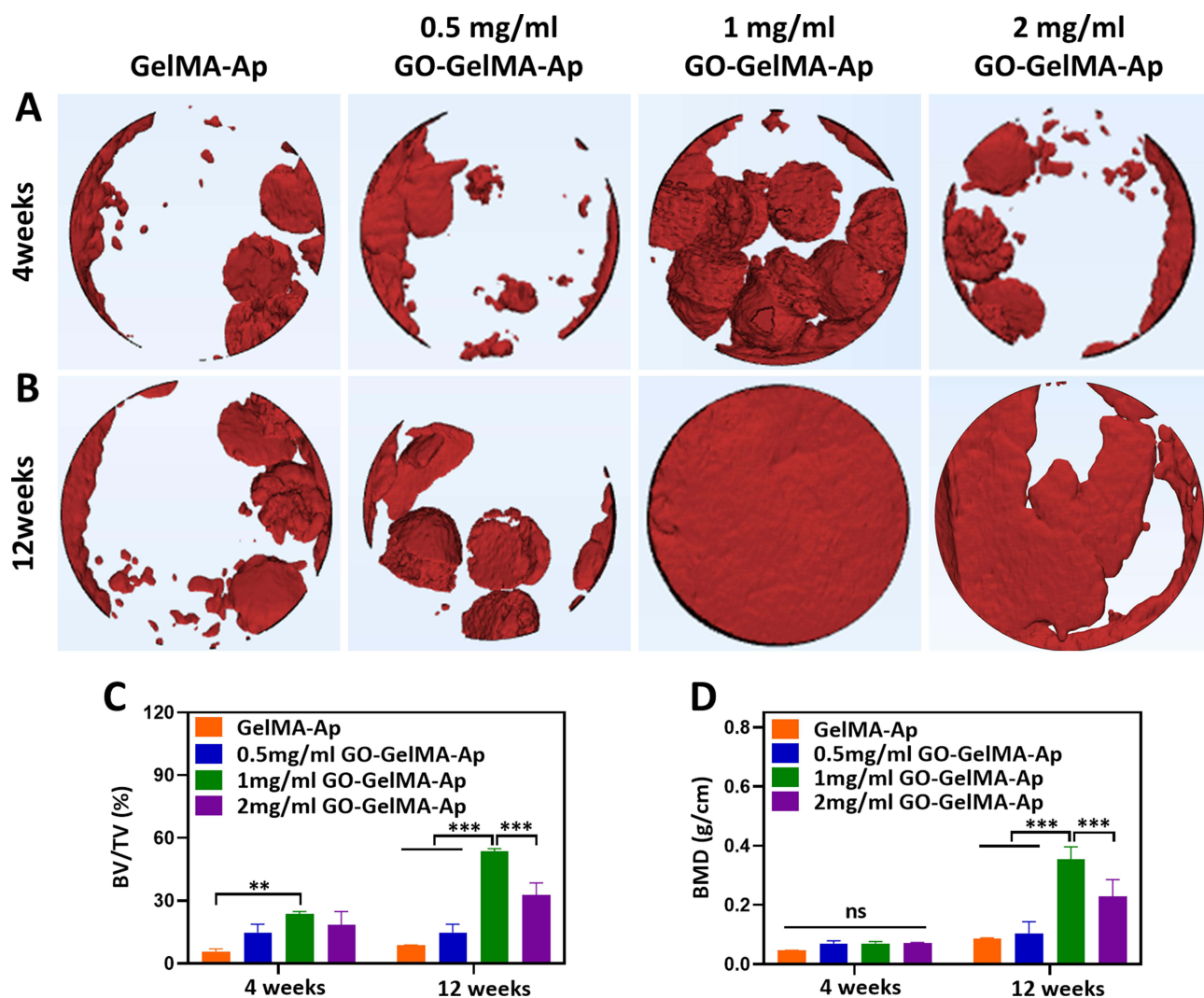
Figure 7 In vivo assessment of the microgels for critical-sized cranial defect in rat. Representative 3D surface reconstruction images of the defect site at week (**A**) 4 and (**B**) 12 post-implantation. Quantitative examination of (**C**) bone tissue volume fraction (BV/TV) and (**D**) bone mineral density (BMD) in the defect site. ** $p < 0.01$, *** $p < 0.001$.

GelMA-Ap microgel was designed in this study, and the optimal GO concentration and immersion time in SBF were explored. The critical-size bone defect was remedied with the implementation of biomimetic GO-GelMA-Ap microgels, thus, confirming the osteoinductive capacity of the microgels in vivo. Furthermore, GO incorporation in GelMA microgels improved the efficacy of the Ap formation process in SBF.

The homogenous distribution of GO in the GO-GelMA microgels resulted in the functional moieties evenly spreaded on the surface.[35] Abundant −COOH and −OH groups in GO offered ample nucleation sites for GelMA microgels in SBF.[36] Given that the sites provided by the GO oxidation group are consumed during binding to the pre-nucleation clusters in the SBF, GO in low concentrations may not create additional nucleation sites. In contrast, a high GO concentration (1 and 2 mg/mL) provided sufficient nucleation sites to accelerate the biomimetic mineration process and form bone-like Ap (Ca/P = 1.66 ± 0.07) with similar characteristics to native bone tissue. Moreover, more mineral deposits and deep mineralization depth were observed on days 3 and 7 of mineralization for 1 mg/mL and 2 mg/mL GO-GelMA-Ap microgel than GelMA-Ap microgel in SEM (Figure 3B). This finding corroborated the GO ability to stimulate biomimetic mineralization of the GelMA microgel. In addition, the Micro-CT results of the four microgels demonstrated that the 1 and 2 mg/mL Go-GelMA-AP group had more hydroxyapatite content and better mineralization in the center and exhibited the largest proportion of Ap volume (Figure 5).
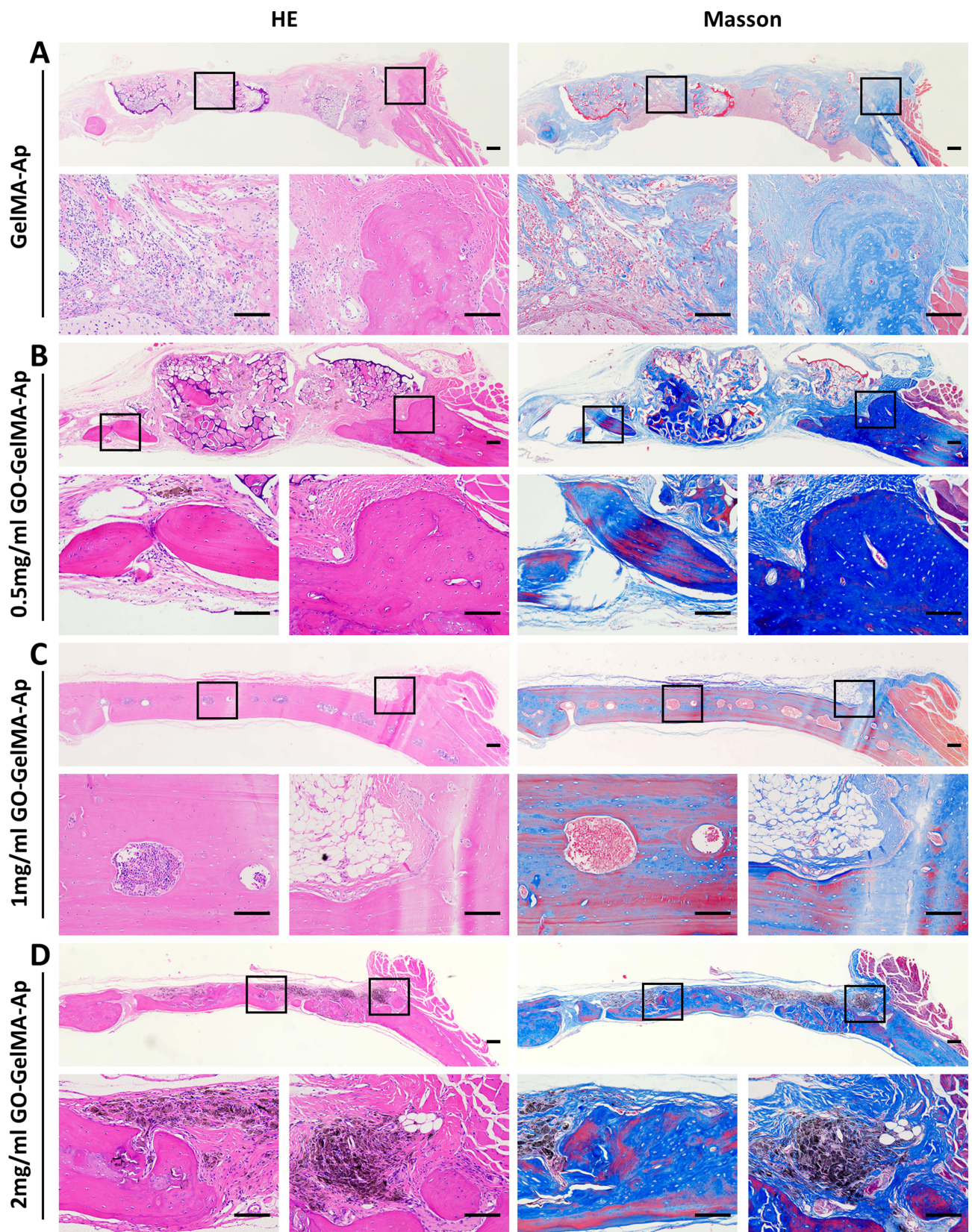
Figure 8 Histological examination of the microgels after implantation for 12 weeks. (**A–D**) H&E staining and Masson's Trichrome staining images of the four group microgels after implantation for 12 weeks, respectively. Scale bar = 200 μm (top), scale bar = 100 μm (below).
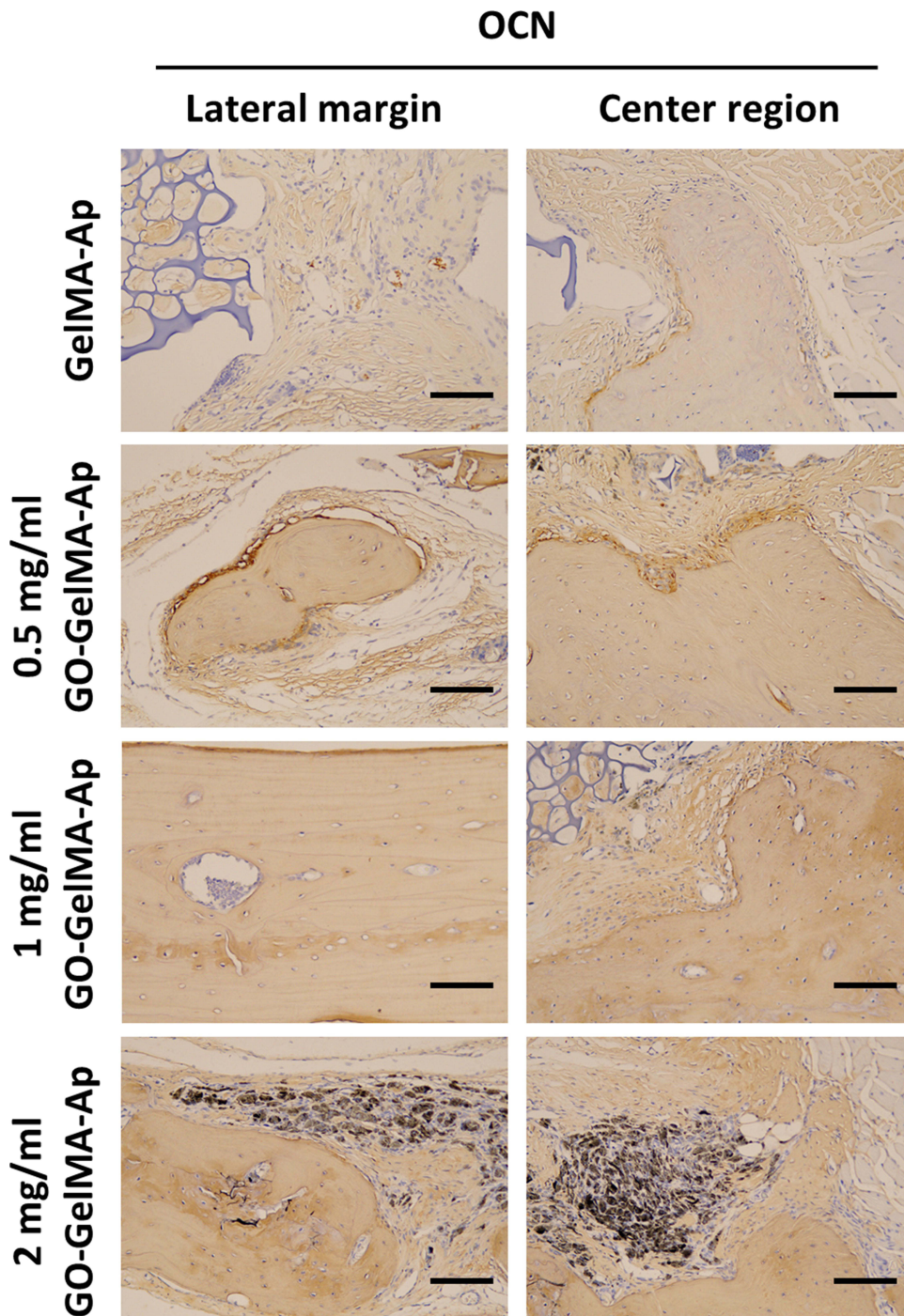
OCN

Figure 9 OCN staining pictures of the microgels after implantation for 12 weeks. Scale bar = 100 μm.

Despite the promising results of GO in bone regeneration, concerns regarding the potential toxicity of this compound remain. Based on the current study findings, the cytotoxicity of GO is associated with size, concentration, functionality, and fabrication structure.[37] The live/dead staining and quantitative assay of living cell numbers in the microgel indicated more live cell growth on the microgel with increasing GO concentration (Figure 6A and C). Therefore, GO did not exhibit adverse effects on cell growth and proliferation. At 12 weeks post-implantation, GO deposition was observed in the defect area without evidence of inflammatory cell infiltration (Figure 8A–D). An earlier study reported that GO could be slowly degraded via

enzymatic and photo-Fenton reactions.[38] In the present study, the 12-week in vivo bone regeneration experiment suggested no biotoxicity in GO-GelMA groups, but a long-term biotoxicity assessment is essential for further GO-GelMA application.

The mechanical performance of bone substitutes is crucial in determining cell fate. Numerous studies have demonstrated that softer matrices are superior for chondrocyte differentiation, while dense matrices are viable for osteogenic differentiation.[39] The elastic modulus of the four microgel groups in this study exceeded 40 kPa, hence, appropriate for cell proliferation. The elastic modulus of the GO-incorporated microgels was higher than the GelMA-Ap microgels, peaking in the 1 and 2 mg/mL GO-GelMA-Ap microgels (Figure 4G). The enhanced mechanical characteristics could be attributed to the non-covalent interaction between GO and the hydrogel.[40] Moreover, GO addition promoted the microgel mineralization efficiency, and higher Ap deposition enhanced the mechanical strength of the microgel.[36]

The cranial bone defect model was established in this study to evaluate the bone regeneration efficacy of microgels (Figures 8 and 9). The findings indicated that the cranial bone defects in the 1 mg/mL GO-GelMA-Ap exhibited a near-complete filling of newly-formed bone tissue after 12 weeks of implantation. In addition, the H&E, Masson's Trichrome, and OCN stainings also suggested that the 1 mg/mL Go-GelMA-Ap microgel was superior in bone repair, besides the extensive new bone formation surrounding the defect area. Firstly, the GO was added to GelMA to create an even structure with thinner and wrinkled pore walls, allowing for faster cell infiltration, adhesion, proliferation, differentiation, ECM formation, and integration with host bone.[41] Secondly, crystallization can be accelerated to a certain extent due to the presence of GO, promoting mineral deposition on the microgel and accelerating osseointegration.[42] Moreover, the mineralized bone-like apatites in GO incorporated microgels improved host-derived cells proliferation and osteogenic differentiation.[43] Finally, recent studies have reported that GO can promote angiogenesis. Angiogenesis is a fundamental process in bone tissue regeneration. The GO could induce angiogenesis and contribute to nutrient formation and transportation in bone regeneration, thus, promoting cell osteogenesis in the microgel.[44]

Conclusion

In summary, we successfully constructed porous GO-GelMA-Ap microgel via chemical crosslinking reactions. This GO-incorporated composite microgel possessed good physiochemical properties, osteoinductivity, and increased biomineralization efficiency than GelMA microgels. Specifically, the optimal GO concentration (1 mg/mL) and SBF immersion time (7 days) were also identified in this study. Finally, the critical-sized rat cerebral defects were repaired using the 1 mg/mL GO-GelMA-Ap microgels. These results suggest that GO-GelMA-Ap microgel could serve as a novel substitute in bone tissue engineering.

Acknowledgments

Author Contributions

All authors involved in analyzing the data, drafting or revising the article, agree to submit the article to the journal and agree to proceed with publication and take responsibility for all aspects of the work.

Funding

Disclosure

The authors declare no competing financial interests.

References

1. Bei HP, Hung PM, Yeung HL, Wang S, Zhao X. Bone-a-petite: engineering exosomes towards bone, osteochondral, and cartilage repair. *Small (Weinheim an der Bergstrasse, Germany)*. 2021;17(50):e2101741. doi:10.1002/smll.202101741

2. Baldwin P, Li DJ, Auston DA, et al. Autograft, allograft, and bone graft substitutes: clinical evidence and indications for use in the setting of orthopaedic trauma surgery. *J Orthop Trauma*. 2019;33:203–213. doi:10.1097/BOT.0000000000001420

3. Schmidt AH. Autologous bone graft: is it still the gold standard? *Injury-Int J Care Inj*. 2021;52:S18–S22. doi:10.1016/j.injury.2021.01.043

4. Mamidi N, Ijadi F, Norahan MH. Leveraging the recent advancements in GelMA scaffolds for bone tissue engineering: an assessment of challenges and opportunities. *Biomacromolecules*. 2023. doi:10.1021/acs.biomac.3c00279

5. Herrera-Ruiz A, Tovar BB, García RG, Tamez MFL, Mamidi N. Nanomaterials-incorporated chemically modified gelatin methacryloyl-based biomedical composites: a novel approach for bone tissue engineering. *Pharmaceutics*. 2022;14:2645. doi:10.3390/pharmaceutics14122645

6. Kurian AG, Mandakhbayar N, Singh RK, et al. Multifunctional dendrimer@nanoceria engineered GelMA hydrogel accelerates bone regeneration through orchestrated cellular responses. *Mater Today Bio*. 2023;20:100664. doi:10.1016/j.mtbio.2023.100664

7. Mamidi N, Velasco Delgadillo RM, Barrera EV, Ramakrishna S, Annabi N. Carbonaceous nanomaterials incorporated biomaterials: the present and future of the flourishing field. *Compos Part B Eng*. 2022;243:110150. doi:10.1016/j.compositesb.2022.110150

8. Yue K, Trujillo-de santiago G, Alvarez M, et al. Synthesis, properties, and biomedical applications of gelatin methacryloyl (GelMA) hydrogels. *Biomaterials*. 2015;73:254–271. doi:10.1016/j.biomaterials.2015.08.045

9. Kurian AG, Singh RK, Patel KD, Lee J, Kim H. Multifunctional GelMA platforms with nanomaterials for advanced tissue therapeutics. *Bioact Mater*. 2022;8:267–295. doi:10.1016/j.bioactmat.2021.06.027

10. Caldwell AS, Aguado BA, Anseth KS. Designing microgels for cell culture and controlled assembly of tissue microenvironments. *Adv Funct Mater*. 2020;30:1907670. doi:10.1002/adfm.201907670

11. Xiao S, Zhao T, Wang J, et al. Gelatin methacrylate (GelMA)-based hydrogels for cell transplantation: an effective strategy for tissue engineering. *Stem Cell Rev Rep*. 2019;15:664–679. doi:10.1007/s12015-019-09893-4

12. Mamidi N, Villela Castrejón J, González-Ortiz A. Rational design and engineering of carbon nano-onions reinforced natural protein nanocomposite hydrogels for biomedical applications. *J Mech Behav Biomed Mater*. 2020;104:103696. doi:10.1016/j.jmbbm.2020.103696

13. Bd H, Zm W, Am A, Sa S. Graphene oxide as a scaffold for bone regeneration. *Wiley Interdiscip Rev Nanomed Nanobiotechnol*. 2017;9:e1437.

14. Purohit SD, Bhaskar R, Singh H, et al. Development of a nanocomposite scaffold of gelatin-alginate-graphene oxide for bone tissue engineering. *Int J Biol Macromol*. 2019;133:592–602. doi:10.1016/j.ijbiomac.2019.04.113

15. Xue H, Zhang Z, Lin Z, et al. Enhanced tissue regeneration through immunomodulation of angiogenesis and osteogenesis with a multifaceted nanohybrid modified bioactive scaffold. *Bioact Mater*. 2022;18:552–568. doi:10.1016/j.bioactmat.2022.05.023

16. He Y, Tian M, Li X, et al. A hierarchical-structured mineralized nanofiber scaffold with osteoimmunomodulatory and osteoinductive functions for enhanced alveolar bone regeneration. *Adv Healthc Mater*. 2022;11. doi:10.1002/adhm.202102236

17. S S, S V, F L, A P, R S. Biosynthesis and characterization of hydroxyapatite and its composite (hydroxyapatite-gelatin-chitosan-fibrin-bone ash) for bone tissue engineering applications. *Int J Biol Macromol*. 2019;129:844–852. doi:10.1016/j.ijbiomac.2019.02.058

18. Singh RK, Yoon DS, Mandakhbayar N, et al. Diabetic bone regeneration with nanoceria-tailored scaffolds by recapitulating cellular microenvironment: activating integrin/TGF-β co-signaling of MSCs while relieving oxidative stress. *Biomaterials*. 2022;288:121732. doi:10.1016/j.biomaterials.2022.121732

19. Singh RK, Jin G-Z, Mahapatra C, et al. Mesoporous silica-layered biopolymer hybrid nanofibrous scaffold: a novel nanobiomatrix platform for therapeutics delivery and bone regeneration. *ACS Appl Mater Interfaces*. 2015;7:8088–8098. doi:10.1021/acsami.5b00692

20. I SS, M R, A BK, D R. Preparation and characterization of polycaprolactone/chitosan-g-polycaprolactone/hydroxyapatite electrospun nanocomposite scaffolds for bone tissue engineering. *Int J Biol Macromol*. 2021;182:1638–1649. doi:10.1016/j.ijbiomac.2021.05.163

21. Kokubo T, Takadama H. How useful is SBF in predicting in vivo bone bioactivity? *Biomaterials*. 2006;27(15):2907–2915. doi:10.1016/j.biomaterials.2006.01.017

22. A J, O J, Z S, D S. Synthesis and applications of graphene oxide. *Materials (Basel, Switzerland)*. 2022;15:920.

23. Sun M, Sun X, Wang Z, et al. Synthesis and properties of gelatin methacryloyl (GelMA) hydrogels and their recent applications in load-bearing tissue. *Polymers*. 2018;10(11):1290. doi:10.3390/polym10111290

24. Matellan C, Del Río Hernández AE. Cost-effective rapid prototyping and assembly of poly(methyl methacrylate) microfluidic devices. *Sci Rep*. 2018;8(1):6971. doi:10.1038/s41598-018-25202-4

25. Mamidi N, Velasco Delgadillo RM, Barrera EV. Covalently functionalized carbon nano-onions integrated gelatin methacryloyl nanocomposite hydrogel containing γ-cyclodextrin as drug carrier for high-performance pH-triggered drug release. *Pharmaceuticals*. 2021;14:291. doi:10.3390/ph14040291

26. Guo Y, Chi X, Wang Y, et al. Mitochondria transfer enhances proliferation, migration, and osteogenic differentiation of bone marrow mesenchymal stem cell and promotes bone defect healing. *Stem Cell Res Ther*. 2020;11:245. doi:10.1186/s13287-020-01704-9

27. Hidayah NMS, Liu WW, Lai CW, et al. Comparison on graphite, graphene oxide and reduced graphene oxide: synthesis and characterization. AIP Conference Proceedings. Vol.1892; 2017.

28. A M, M P, T G. A review on bovine hydroxyapatite; extraction and characterization. *Biomed Phys Eng Express*. 2021;8:012001.

29. Boota M, Ahmad I, Ahmad J. Production of graphene-derivatives using organic molecules for supercapacitors and beyond. *Colloids Surf A Physicochem Eng Asp*. 2023;658:130693. doi:10.1016/j.colsurfa.2022.130693

30. Wang J, Wu D, Zhang Z, et al. Biomimetically ornamented rapid prototyping fabrication of an apatite-collagen-polycaprolactone composite construct with nano-micro-macro hierarchical structure for large bone defect treatment. *ACS Appl Mater Interfaces*. 2015;7:26244–26256. doi:10.1021/acsami.5b08534

31. Grazioli G, Silva AF, Souza JF, et al. Synthesis and characterization of poly(vinyl alcohol)/chondroitin sulfate composite hydrogels containing strontium-doped hydroxyapatite as promising biomaterials. *J Biomed Mater Res Part A*. 2021;109:1160–1172. doi:10.1002/jbm.a.37108

32. Wang Q, Liu Z. Study on graphene oxide thermogravimetric method. *Mater Sci*. 2021;11:83–87. doi:10.12677/MS.2021.112011

33. H Z, Fu Q-W, Sun T-W, et al. Amorphous calcium phosphate, hydroxyapatite and poly(d,l-lactic acid) composite nanofibers: electrospinning preparation, mineralization and in vivo bone defect repair. *Colloids Surf B Biointerfaces*. 2015;136:27–36. doi:10.1016/j.colsurfb.2015.08.015

34. Sugimoto K, Zhou Y, Galindo T, Kimura R, Tagaya M. Investigation of surface layers on biological and synthetic hydroxyapatites based on bone mineralization process. *Biomimetics (Basel, Switzerland)*. 2023;8. doi:10.3390/biomimetics8020184

35. P Z, M A, A S, Z B, Am S. Graphene oxide: opportunities and challenges in biomedicine. *Nanomaterials (Basel, Switzerland)*. 2021;11:1083.

36. Jiang Y, Zhou D, Yang B. 3D bioprinted GelMA/GO composite induces osteoblastic differentiation. *J Biomater Appl*. 2022;37:527–537. doi:10.1177/08853282221098235

37. Rhazouani A, Gamrani H, Ed-Day S, et al. Sub-acute toxicity of graphene oxide (GO) nanoparticles in male mice after intraperitoneal injection: behavioral study and histopathological evaluation. *Food Chem Toxicol*. 2023;171:113553. doi:10.1016/j.fct.2022.113553

38. Vlasova II, Kapralov AA, Michael ZP, et al. Enzymatic oxidative biodegradation of nanoparticles: mechanisms, significance and applications. *Toxicol Appl Pharmacol*. 2016;299:58–69. doi:10.1016/j.taap.2016.01.002

39. Žigon-branc S, Markovic M, Van Hoorick J, et al. Impact of hydrogel stiffness on differentiation of human adipose-derived stem cell microspheroids. *Tissue Eng Part A*. 2019;25:1369–1380. doi:10.1089/ten.tea.2018.0237

40. Bao J, Qin W, Zhu Q, Qian WH. Enhanced mechanical properties and cytocompatibility of GelMA hydrogels by incorporating graphene oxide. *Shanghai J Stomatol*. 2022;31:491–496.

41. Ignat SR, Lazăr AD, Şelaru A, et al. Versatile biomaterial platform enriched with graphene oxide and carbon nanotubes for multiple tissue engineering applications. *Int J Mol Sci*. 2019;20. doi:10.3390/ijms20163868

42. Kumari S, Singh D, Srivastava P, Singh BN, Mishra A. Generation of graphene oxide and nano-bioglass based scaffold for bone tissue regeneration. *Biomedical Materials (Bristol, England)*. 2022;17. doi:10.1088/1748-605X/ac92b4

43. Bayaraa O, Dashnyam K, Singh RK, et al. Nanoceria-GO-intercalated multicellular spheroids revascularize and salvage critical ischemic limbs through anti-apoptotic and pro-angiogenic functions. *Biomaterials*. 2023;292:121914. doi:10.1016/j.biomaterials.2022.121914

44. Xue D, Chen E, Zhong H, et al. Immunomodulatory properties of graphene oxide for osteogenesis and angiogenesis. *Int J Nanomed*. 2018;13:5799–5810. doi:10.2147/IJN.S170305